Elastic modeling of surface waves

Gustavo Alves

ABSTRACT

I implement a free surface boundary condition for the generation of surface waves using a 10^{th} order in space and 2^{nd} order in time finite-difference staggered-grid scheme. I show an example of a field seismic section and recreate its main features using the proposed scheme. The synthetic data created show Rayleigh waves, backscattered waves and mode conversions, and fit the kinematics of the field data.

INTRODUCTION

Surface waves appear whenever the interface between two elastic media can be described as a free surface, i.e., a boundary that exhibits null stress components acting on the plane of the interface (Takeuchi and Saito, 1972). In seismology, this condition is observed in ground-to-air and sea floor interfaces. Therefore, surface waves are ubiquitous in seismic land data and increasingly more common in marine data with the advent of sea bottom receivers like ocean bottom cables (OBCs) and ocean bottom nodes (OBNs) (Boiero et al., 2013).

In seismic data, surface waves are observed as slow, dispersive linear high wavenumber events and are usually considered coherent noise that needs to be either filtered or muted out (Boustani et al., 2013). However, they contain important information about the elastic properties of the shallow layers of the subsurface and could give hints into their understanding. This makes surface wave modeling an interesting and yet understudied subject in seismic.

In Alves and Biondi (2014), I focused in the implementation of a finite-difference staggered-grid method for modeling elastic waves. That work was based on the work of Virieux (1986) and followed the algorithm later proposed by Ikelle and Amundsen (2005). Here, I extend the previous work, adding a free-surface boundary condition that allows the generation of surface waves. The methodology still follows that presented in Ikelle and Amundsen (2005), but the spatial derivative stencils used are 10^{th} order. In the next section, I present the changes to the implementation adopted to achieve this higher order boundary condition.

Finally, I compare a field seismic section and an equivalent synthetic data set generated using the proposed algorithm.

METHOD

The introduction of a free surface in the elastic finite-difference code imposes a non-slipping contact and null stresses at the boundary, thus satisfying the continuity relations for strain and stress. I implement these boundary conditions in a 10^{th} order stencil using the method of mirror images, similarly to the 4^{th} order implementation described in Ikelle and Amundsen (2005). However, due to the longer stencil, the method of mirror images must be applied gradually as the differential equation is evaluated at different distances from the free surface. Equations 1 through 4 describe the normal stress calculated at the grid points close to the boundary at a fixed time step. For the solution shown here, the free surface is located at $z = 1$ and the indeces correspond to the grid positions where the properties are evaluated:

$$\begin{aligned}
\tau_{zz}(x,1) &= \frac{\Delta t}{\Delta x}((\lambda(x,1)+2\mu(x,1))\times \\
&(\; c_1 \; (V_z(x,6)+V_z(x,4)) \\
&+ \; c_2 \; (V_z(x,5)+V_z(x,3)) \\
&+ \; c_3 \; (V_z(x,4)+V_z(x,2)) \\
&+ \; c_4 \; (V_z(x,3)+V_z(x,1)) \\
&+ \; c_5 \; (V_z(x,2)-V_z(x,1))) \\
&+ \quad \lambda(x,1)\times \\
&(\; c_1 \; (V_x(x+5,1)-V_x(x-4,1)) \\
&+ \; c_2 \; (V_x(x+4,1)-V_x(x-3,1)) \\
&+ \; c_3 \; (V_x(x+3,1)-V_x(x-2,1)) \\
&+ \; c_4 \; (V_x(x+2,1)-V_x(x-1,1)) \\
&+ \; c_5 \; (V_x(x+1,1)-V_x(x,1)))); \qquad (1)
\end{aligned}$$

$$\begin{aligned}
\tau_{zz}(x,2) &= \frac{\Delta t}{\Delta x}((\lambda(x,2)+2\mu(x,2))\times \\
&(\; c_1 \; (V_z(x,7)+V_z(x,3)) \\
&+ \; c_2 \; (V_z(x,6)+V_z(x,2)) \\
&+ \; c_3 \; (V_z(x,5)+V_z(x,1)) \\
&+ \; c_4 \; (V_z(x,4)-V_z(x,1)) \\
&+ \; c_5 \; (V_z(x,3)-V_z(x,2))) \\
&+ \quad \lambda(x,2)\times \\
&(\; c_1 \; (V_x(x+5,1)-V_x(x-4,1)) \\
&+ \; c_2 \; (V_x(x+4,1)-V_x(x-3,1)) \\
&+ \; c_3 \; (V_x(x+3,1)-V_x(x-2,1)) \\
&+ \; c_4 \; (V_x(x+2,1)-V_x(x-1,1)) \\
&+ \; c_5 \; (V_x(x+1,1)-V_x(x,1)))); \qquad (2)
\end{aligned}$$

$$
\begin{aligned}
\tau_{zz}(x,3) &= \frac{\Delta t}{\Delta x}((\lambda(x,3)+2\mu(x,3))\times \\
&(\quad c_1 \quad (V_z(x,8)+V_z(x,2)) \\
&+ \quad c_2 \quad (V_z(x,7)+V_z(x,1)) \\
&+ \quad c_3 \quad (V_z(x,6)-V_z(x,1)) \\
&+ \quad c_4 \quad (V_z(x,5)-V_z(x,2)) \\
&+ \quad c_5 \quad (V_z(x,4)-V_z(x,3))) \\
&+ \qquad \lambda(x,3)\times \\
&(\quad c_1 \quad (V_x(x+5,1)-V_x(x-4,1)) \\
&+ \quad c_2 \quad (V_x(x+4,1)-V_x(x-3,1)) \\
&+ \quad c_3 \quad (V_x(x+3,1)-V_x(x-2,1)) \\
&+ \quad c_4 \quad (V_x(x+2,1)-V_x(x-1,1)) \\
&+ \quad c_5 \quad (V_x(x+1,1)-V_x(x,1)))); \qquad (3)
\end{aligned}
$$

$$
\begin{aligned}
\tau_{zz}(x,4) &= \frac{\Delta t}{\Delta x}((\lambda(x,4)+2\mu(x,4))\times \\
&(\quad c_1 \quad (V_z(x,9)+V_z(x,1)) \\
&+ \quad c_2 \quad (V_z(x,8)-V_z(x,1)) \\
&+ \quad c_3 \quad (V_z(x,7)-V_z(x,2)) \\
&+ \quad c_4 \quad (V_z(x,6)-V_z(x,3)) \\
&+ \quad c_5 \quad (V_z(x,5)-V_z(x,4))) \\
&+ \qquad \lambda(x,3)\times \\
&(\quad c_1 \quad (V_x(x+5,1)-V_x(x-4,1)) \\
&+ \quad c_2 \quad (V_x(x+4,1)-V_x(x-3,1)) \\
&+ \quad c_3 \quad (V_x(x+3,1)-V_x(x-2,1)) \\
&+ \quad c_4 \quad (V_x(x+2,1)-V_x(x-1,1)) \\
&+ \quad c_5 \quad (V_x(x+1,1)-V_x(x,1)))), \qquad (4)
\end{aligned}
$$

where $\tau_{zz}(x,z)$ is the normal stress component in the z direction; V_x and V_z are the particle displacements in the x and z directions, respectively; and $\lambda(x,z)$ and $\mu(x,z)$ are the Lamé parameters. Equation 5 shows the values of c_1 to c_5, which correspond to the 10^{th} order finite-difference coefficients, according to Liu and Sen (2009).

$$\begin{aligned} c_1 &= \frac{35}{294912}, \\ c_2 &= -\frac{405}{229376}, \\ c_3 &= \frac{567}{40960}, \\ c_4 &= -\frac{735}{8192}, \\ c_5 &= \frac{19845}{16384}. \end{aligned} \tag{5}$$

The equations for the horizontal stress can be obtained by swapping the $(\lambda(x,z)+2\mu(x,z))$ and $\lambda(x,z)$ terms in Equations 1 through 4. For the shear stress τ_{xz}, the derivatives of the displacement field are shown on Equations 6 through 10. Continuity of the physical parameters requires the shear stress be null exactly at the boundary at $z=1$. The coefficients for the 10^{th} order stencil are the same as in the previous set of equations.

$$\tau_{xz}(x,1) = 0 \tag{6}$$

$$\begin{aligned} \tau_{xz}(x,2) &= \frac{\Delta t}{\Delta x}((\mu(x,2)) \times \\ &(\quad c_1 \quad (V_x(x,6)+V_x(x,4)) \\ &+ \quad c_2 \quad (V_x(x,5)+V_x(x,3)) \\ &+ \quad c_3 \quad (V_x(x,4)+V_x(x,2)) \\ &+ \quad c_4 \quad (V_x(x,3)+V_x(x,1)) \\ &+ \quad c_5 \quad (V_x(x,2)-V_x(x,1)) \\ &+ \quad c_1 \quad (V_z(x+4,2)-V_z(x-5,2)) \\ &+ \quad c_2 \quad (V_z(x+3,2)-V_z(x-4,2)) \\ &+ \quad c_3 \quad (V_z(x+2,2)-V_z(x-3,2)) \\ &+ \quad c_4 \quad (V_z(x+1,2)-V_z(x-2,2)) \\ &+ \quad c_5 \quad (V_z(x,2)-V_z(x-1,2)))), \end{aligned} \tag{7}$$

$$\begin{aligned}
\tau_{xz}(x,3) &= \frac{\Delta t}{\Delta x}((\mu(x,3)) \times \\
&(\quad c_1 \quad (V_x(x,7) + V_x(x,3)) \\
&+ \quad c_2 \quad (V_x(x,6) + V_x(x,2)) \\
&+ \quad c_3 \quad (V_x(x,5) + V_x(x,1)) \\
&+ \quad c_4 \quad (V_x(x,4) - V_x(x,1)) \\
&+ \quad c_5 \quad (V_x(x,3) - V_x(x,2)) \\
&+ \quad c_1 \quad (V_z(x+4,3) - V_z(x-5,3)) \\
&+ \quad c_2 \quad (V_z(x+3,3) - V_z(x-4,3)) \\
&+ \quad c_3 \quad (V_z(x+2,3) - V_z(x-3,3)) \\
&+ \quad c_4 \quad (V_z(x+1,3) - V_z(x-2,3)) \\
&+ \quad c_5 \quad (V_z(x,3) - V_z(x-1,3)))),
\end{aligned} \tag{8}$$

$$\begin{aligned}
\tau_{xz}(x,4) &= \frac{\Delta t}{\Delta x}((\mu(x,4)) \times \\
&(\quad c_1 \quad (V_x(x,8) + V_x(x,2)) \\
&+ \quad c_2 \quad (V_x(x,7) + V_x(x,1)) \\
&+ \quad c_3 \quad (V_x(x,6) - V_x(x,1)) \\
&+ \quad c_4 \quad (V_x(x,5) - V_x(x,2)) \\
&+ \quad c_5 \quad (V_x(x,4) - V_x(x,3)) \\
&+ \quad c_1 \quad (V_z(x+4,4) - V_z(x-5,4)) \\
&+ \quad c_2 \quad (V_z(x+3,4) - V_z(x-4,4)) \\
&+ \quad c_3 \quad (V_z(x+2,4) - V_z(x-3,4)) \\
&+ \quad c_4 \quad (V_z(x+1,4) - V_z(x-2,4)) \\
&+ \quad c_5 \quad (V_z(x,4) - V_z(x-1,4)))),
\end{aligned} \tag{9}$$

$$\begin{aligned}
\tau_{xz}(x,5) &= \frac{\Delta t}{\Delta x}((\mu(x,5)) \times \\
&(\quad c_1 \quad (V_x(x,9) + V_x(x,1)) \\
&+ \quad c_2 \quad (V_x(x,8) - V_x(x,1)) \\
&+ \quad c_3 \quad (V_x(x,7) - V_x(x,2)) \\
&+ \quad c_4 \quad (V_x(x,6) - V_x(x,3)) \\
&+ \quad c_5 \quad (V_x(x,5) - V_x(x,4)) \\
&+ \quad c_1 \quad (V_z(x+4,5) - V_z(x-5,5)) \\
&+ \quad c_2 \quad (V_z(x+3,5) - V_z(x-4,5)) \\
&+ \quad c_3 \quad (V_z(x+2,5) - V_z(x-3,5)) \\
&+ \quad c_4 \quad (V_z(x+1,5) - V_z(x-2,5)) \\
&+ \quad c_5 \quad (V_z(x,5) - V_z(x-1,5)))).
\end{aligned} \tag{10}$$

It is important to note that the spatial derivatives calculated from the displacements are not centered at the same indices as the stress components. That is due to the staggered grid method, which prescribes different postions in the modeling domain for the displacements, stresses and elastic parameters, according to Virieux (1986).

The equations for the displacements in the x and z directions for the grid points near the free surface can be calculated in a similar fashion and will not be shown here.

RESULTS

The method was used to create a 2D synthetic common shot gather that simulated a field shot gather. The example was taken from Claerbout (2011) and contains surface related events such as ground roll and backscattered waves from what appears to be a near-surface anomaly.

Figures 1(a) and 1(b) show the field data and synthetic data, respectively. The field data common-shot gather shows (A) hyperbolic events due to reflections within a thin shallow layer, (B) high amplitude dispersive surface waves (ground roll) and (C) backscattered waves created by a near surface discontinuity. It is also possible to see forward scattered converted waves from the same discontinuity. In the synthetic example, the same events are observed and with the same kinematics. The hyperbolas at the top are much weaker in the synthetic example, due to a very strong contrast inside the low velocity layer. The dynamics of the example could be improved by manually adjusting the model properties.

The elastic parameters used to create the synthetic data emulate a free surface over a low velocity layer with steeply increasing shear velocities in the vertical direction and a near surface scatterer at $x = 250m$. Figures 2(a), 2(b) and 2(c) show the models for V_p, V_s and ρ, respectively. The modeling parameters are $\Delta x = \Delta z = 0.5m$ and $\Delta t = 3.27 \times 10^{-5}$. I used an explosive source with a peak frequency of 25 Hz. Although these grid parameters are finer than those usually employed in finite difference modeling at this frequency, they are required to avoid numerical dispersion of the slower surface modes.

DISCUSSION

A free-surface boundary condition was successfully implemented for a 10^{th} order in space and 2^{nd} order in time finite-difference stencil. The results show that the algorithm correctly recreates surface waves and that they are kinematically similar to those observed in a field data gather. The dynamics of the field data appear to have been reproduced, although a better correspondence might be achieved if an elastic model for the field data was available.

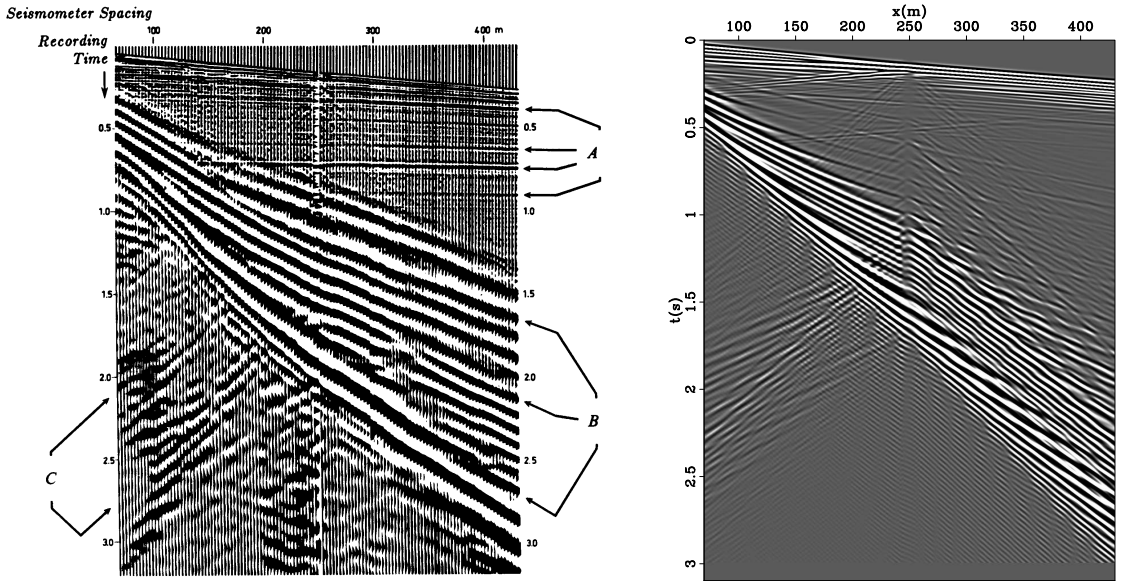

(a) (b)

Figure 1: (a) 2D field data and (b) synthetic data. The events marked as A, B and C correspond to primaries, ground roll and backscattered waves, respectively. Kinematically, there is a good match between the events observed in each gather, including the mode conversions from P to S waves at $x = 250m$. [**NR**] [**ER**]

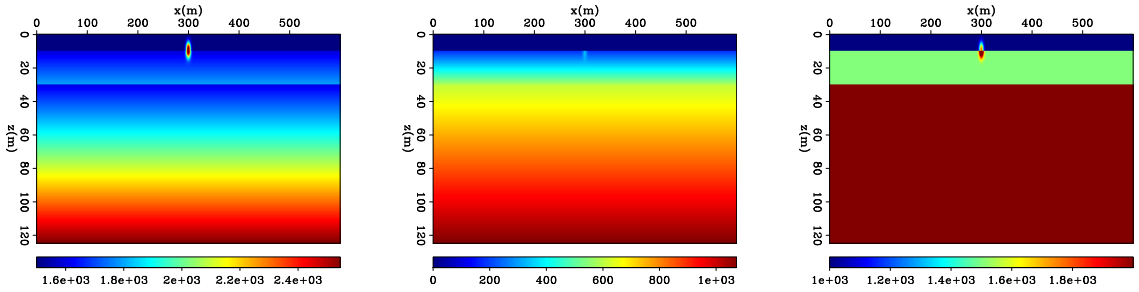

(a) (b) (c)

Figure 2: (a)V_p, (b) V_s and (c) ρ models. [**ER**]

Due to the slower speeds of propagation for surface waves, the spatial sampling of the model was refined to avoid numerical dispersion. Consequently, the time sampling of the modeling must also be refined to maintain numerical stability.

ACKNOWLEDGMENT

I would like to thank the Stanford Exploration Project sponsors for the ongoing support and Petrobras for support of my PhD.

REFERENCES

Alves, G. and B. Biondi, 2014, High-order elastic finite-difference modeling: Stanford Exploration Project Report, **152**, 327–340.

Boiero, D., E. Wiarda, and P. Vermeer, 2013, Surface-and guided-wave inversion for near-surface modeling in land and shallow marine seismic data: The Leading Edge, **32**, 638–646.

Boustani, B., S. Torabi, A. Javaherian, and S. A. Mortazavi, 2013, Ground roll attenuation using a curvelet-svd filter: a case study from the west of iran: Journal of Geophysics and Engineering, **10**, 055006.

Claerbout, J. F., 2011, Basic earth imaging.

Ikelle, L. and L. Amundsen, 2005, Introduction to petroleum seismology: Society of Exploration Geophysicists Tulsa, OK.

Liu, Y. and M. K. Sen, 2009, An implicit staggered-grid finite-difference method for seismic modelling: Geophysical Journal International, **179**, 459–474.

Takeuchi, H. and M. Saito, 1972, Seismic surface waves: Methods in computational physics, **11**, 217–295.

Virieux, J., 1986, P-SV wave propagation in heterogeneous media: Velocity-stress finite-difference method: Geophysics, **51**, 889–901.